Jpn. J. Cancer Res. **93**, 259–266, March 2002

Three-dimensional Reconstruction and Fractal Geometric Analysis of Serrated Adenoma

Masahiro Iwabuchi,[1,2] Mareyuki Endoh,[1] Nobuo Hiwatashi,[2] Yoshitaka Kinouchi,[2] Tooru Shimosegawa,[2] Takayuki Masuda,[3] Takuya Moriya[1] and Hironobu Sasano[1]

Departments of [1]Pathology and [2]Gastroenterology, Tohoku University Graduate School of Medicine and [3]College of Medical Sciences, Tohoku University, 1-1 Seiryo-machi, Aoba-ku, Sendai 980-8574

Serrated adenoma (SA) is a relatively newly defined entity of colorectal neoplasm first characterized by Longacre and Fenoglio-Preiser in 1990. This lesion is characterized by a complicated serrated edge of crypts. In this study, we performed three-dimensional (3-D) reconstruction, including 3-D distribution patterns of Ki-67-positive cells and fractal dimension of SA, in order to evaluate the nature of the complicated architecture, including its possible morphogenesis. We studied nine colonoscopic polypectomy specimens including three SAs, three tubular adenomas (TAs), and three hyperplastic polyps (HPs). Sixty serial tissue sections per case were stained alternately with hematoxylin and eosin (H&E) and Ki-67 immunostain. Each serial image was then digitized for 3-D computer analysis and the distribution pattern of Ki-67-positive cells was evaluated. Ki-67-immunostained sections were also subjected to 2-D quantitative morphometric study. In addition, the fractal dimensions of images from H&E-stained sections were examined using a box-counting method. Results of the 3-D reconstruction study demonstrated that glandular budding and branching were more frequent in SA than in TA or HP. These findings were confirmed quantitatively by the results of fractal geometric analysis of these polyps (fractal dimension:1.34±0.08 for SA, 1.23±0.07 for TA, and 1.28±0.12 for HP). Ki-67-positive cells in HP were localized mainly in the bottom of crypts and those in TA were diffusely distributed, while Ki-67-positive cells in SA were mainly aggregated in the depressed sites of serrated epithelia. These findings were also confirmed quantitatively using 2-D morphometry. These distribution patterns of the proliferative zone of SA are considered to contribute to the formation of the characteristic serrated epithelia and the complicated morphological appearance of SA.

Key words: Serrated adenoma — Three-dimensional reconstruction — Fractal dimension

Benign colorectal epithelial polyps have been classified into two histological subtypes: hyperplastic polyp and adenoma.[1–4] Hyperplastic polyp is characterized by a serrated epithelium with goblet cell hypertrophy without cytological or nuclear atypia,[5] whereas colorectal adenoma is composed of closely packed tubules containing incompletely differentiated columnar cells with thin pencil-shaped stratified nuclei.[2] Serrated adenoma (SA) is a relatively new morphological subtype of colorectal adenoma which was first reported by Longacre and Fenoglio-Preiser in 1990.[6] SA is associated with both the architectural features of a hyperplastic polyp and the cytologic features of an adenoma. However, Watanabe[7] from our department had reported the same lesion as "H-type" adenomatous polyp in the 1970's. The unique histological features of this lesion and its possible malignant potential have resulted in a recent increased awareness of SA among gastroenterologists and surgical pathologists.[8–10] However, morphological studies of this lesion, especially with relation to the formation of serrated epithelia and the differences from tubular adenoma (TA) or hyperplastic polyp (HP), have not been fully delineated. Therefore, in this study, we employed the following four different morphometric analyses in order to study the complicated morphological features of SA, and its possible morphogenesis. The purpose of this study was to clarify the structural characteristics of SA and to facilitate an understanding of its biological features. First, we reconstructed the 3-dimensional (3-D) structure of SA from serial 2-D tissue sections employing high-quality microtome knives and 3-D computer graphics software.[11, 12] Previous studies demonstrated that the proliferative zone in HP is confined to the lower two-thirds of the crypts,[13] and that in TA is either present in the upper third or scattered along the whole axis of the crypts and in the surface epithelium.[13, 14] However, the distribution pattern of the proliferative zone in SA has not been fully evaluated. Therefore, we then studied the Ki-67 distribution pattern using a 3-D reconstruction system. In addition, we examined the spatial distribution patterns of Ki-67-positive cells using 2-D morphometric analysis in SA.

Fractal geometry is a useful tool for evaluating the irregular and ordered shapes of many natural objects possessing a fractal structure.[15] The mathematical definition

E-mail: iwabuchi@patholo2.med.tohoku.ac.jp

of a fractal structure is an object which has a fractal dimension greater than its topological dimension,[15] but subjective identification of the property of scaling self-similarity (smaller copies of the complete object present within the bounds of the whole object) usually correlates with this definition.[16] Cross *et al.*[17] reported that colorectal polyps had a fractal structure and that the fractal dimension was significantly different among histopathologically different diagnostic categories, but, to date, the fractal dimension of SA has not been studied. Therefore, we examined the morphological complexity of SA quantitatively using this fractal dimension in our study.

MATERIALS AND METHODS

Tissue samples Three HPs (0.6, 0.6, 2.0 cm in diameter) (Fig. 1), three TAs with low-grade dysplasia (0.8, 0.8, 1.0 cm in diameter) (Fig. 2), and three SAs (0.7, 1.0, 1.7 cm in diameter) (Fig. 3) were examined for 3-D reconstruction. In this study, the criteria of SA were as follows: glandular lumen serration, the presence of goblet cell immaturity, upper zone mitosis, marked nuclear pseudostratification, and the absence of a thickened collagen table.[6] These materials were obtained from colonoscopic polypectomy specimens. Tissue sections were all fixed in 10% formalin for 24–48 h at room temperature and embedded in paraffin wax. From each block, more than 60 serial microscopic sections of 3 μm in thickness were prepared and stained alternately with hematoxylin and eosin (H&E) stain and Ki-67 immunostain for 3-D reconstruction.

In addition, H&E-stained paraffin sections of 27 SAs (0.5–3.7 cm, mean size 1.1 cm), 19 TAs (0.7–2.0 cm, mean size 1.1 cm), and 15 HPs (0.5–2.0 cm, mean size 0.9 cm) were examined for fractal geometrical analyses.

Immunohistochemistry Monoclonal antibodies against Ki-67 (MIB-1) were purchased from Immunotech (Mar-

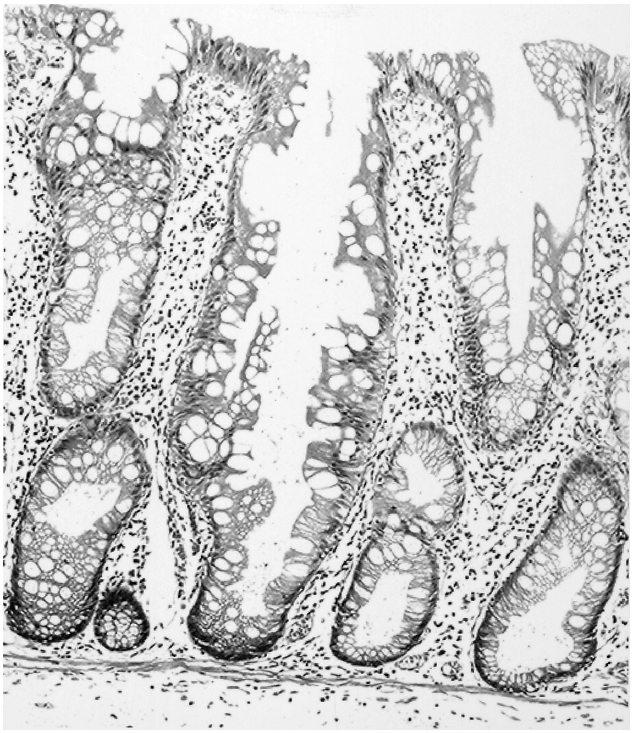

Fig. 1. Histopathologic features of hyperplastic polyp (H&E stain ×50). Luminal serration is observed, but cytological or nuclear atypia is rarely observed.

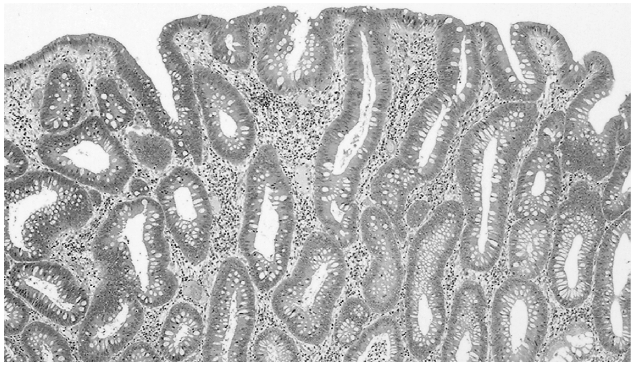

Fig. 2. Histopathologic features of tubular adenoma (H&E stain ×50). The glandular lumens are round to oval, and thin, penicillate, pseudostratified nuclei are observed.

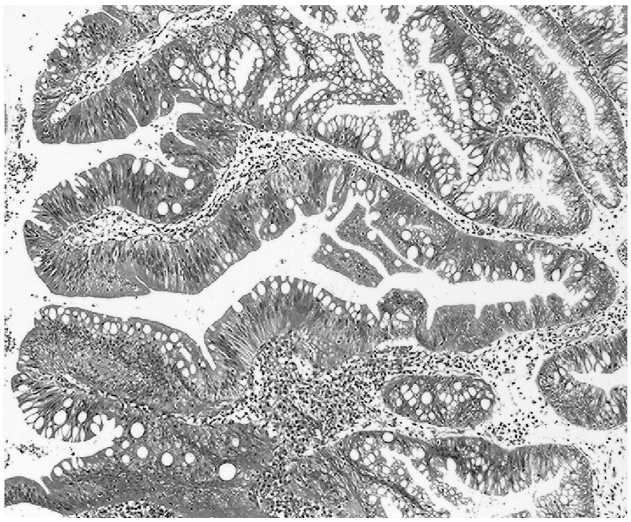

Fig. 3. Histopathologic features of serrated adenoma (H&E stain ×50). Serrated epithelium and pseudostratified nuclei are observed.

seilles, France). Thin (3 μm) slices from paraffin-embedded specimens were deparaffinized routinely. Autoclave treatment at 120°C for 5 min was then employed for antigen retrieval. After the slides had been kept for 1 h at room temperature, they were immersed in a solution of ethanol and 0.3% hydrogen peroxide for 30 min to block endogenous peroxidase activity. Sections were then washed three times (5 min each) with 0.01 mol/liter phosphate-buffered saline (PBS) and treated with 1% normal rabbit serum for 30 min at room temperature. After having been washed, the slides were incubated with primary antibodies for 18 h at 4°C in a humidified chamber. Optimal dilution was 1:50. A Histofine Kit (Nichirei Co., Tokyo) was used in the immunostaining. After washing, the slides were incubated for 30 min at room temperature with biotinylated rabbit anti-mouse immunoglobulin, washed again, and then incubated for 30 min with peroxidase-conjugated streptavidin. The final wash was followed by immersion of the slides for 3 to 5 min in a solution containing 3,3′-diaminobenzidine (0.06 mmol/liter) and hydrogen peroxide (2 mmol/liter), in Tris-HCl (0.05 mol/liter, buffered at pH 7.6). Sections were counterstained with 1% methyl green and mounted in a glycerol gelatin water-soluble medium. The negative control for immunostaining was PBS (0.01 mol/liter), or normal mouse IgG instead of the primary antibodies. Immunoreactivity was not observed in these tissue sections.

3-D reconstruction Serial sections were submitted to computer-aided 3-D graphic reconstruction to visualize the structure of the crypts, as well as the distribution of Ki-67-positive cells and its relationship with the morphogenesis of SA. In the first of a set of serial sections, an area, including several crypts of the polyp in the H&E-stained section, was selected for reconstruction. Using a profile projector (model V-16C; Nikon, Tokyo), the area was projected onto a sheet of tracing paper at a magnification of ×200, and the contours of both the apical and basal membrane contained in the area were faithfully delineated. This procedure was repeated sequentially for every three sections. In addition, Ki-67 immunostaining was also performed every three sections. The images were directly captured through a digital CCD camera (ProgRes 3012 PPC, Kronton Electronic Co., Ltd., Encring, Germany) with a PRI-Macintosh interface board attached to an operating light microscope (Carl Zeiss Co., Ltd., Jena, Germany). Resolution was set at 998×774 pixels. The images were subsequently transferred to a Power Macintosh G3 personal computer and processed with Adobe Photoshop 3.0 J software (Adobe Systems, Inc., San Jose, California). The images were then color-printed and enlarged to A4 (29.6×21.0 cm) size using Pictorography 3000 (Fujix, Tokyo).

The serial pictures produced, as described above, were successively placed on a digitizer, and profiles were inputted into a 3-D reconstruction program (OZ95, 3D reconstruct system version 2.1, Rise Co., Sendai) by tracing with a cursor. On inputting the data, the contours of apical and basal membranes and Ki-67-positive cells were stored as separate files. When all the pictures had been inputted, the computer generated a 3-D picture.

2-D morphometry for analyzing the distribution pattern of Ki-67-positive cells 2-D morphometry of SA cases was conducted to confirm quantitatively that Ki-67-positive cells in SA aggregate in depressed sites of the serrated epithelium. We designed the following new method for the purpose.

Images of Ki-67-immunostained sections of SA at a magnification of ×100 were captured and then color-printed and enlarged to A4 (29.6×21.0 cm) size, as described above. From the basal membrane to the apical membrane, we drew lines vertically at regular intervals on the basal membrane and measured the distance between the basal and apical membranes. Ki-67 positive and negative cells included on the line were then counted. We compared the frequency distribution between the two groups (Fig. 4).

Fractal geometric analysis The fractal dimension of the histological specimens was measured utilizing a box-counting method, as described previously.[16, 18–20] Briefly, the objective shape is divided into square boxes with the size d. The number of boxes: $N(d)$ covering the shape is counted. When d varied, the effective fractal dimension D was subsequently determined from the following relation: $N(d) \in d^{-D}$. A log-log graph is used to calculate the box-counting fractal dimension. The fractal dimension D was obtained from the negative slope of the linear part of the log-log plot. The upper and lower parts of the log-log plot usually flatten and descend.

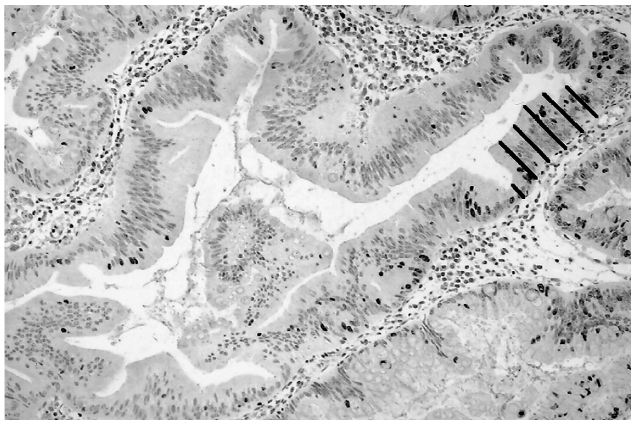

Fig. 4. Vertical lines are drawn at regular intervals and the distance is measured between the basal and apical membrane. Ki-67-positive and negative cells included on the lines are counted, respectively.

The area, including several crypts of the polyp, in the H&E-stained section, was selected for fractal geometric analysis. Using a profile projector (model V-16C; Nikon), the area was projected onto a sheet of tracing paper at a magnification of ×200, and the contours of the apical membrane contained in that area were faithfully delineated. The pictures produced from this tracing were placed on a digitizer, and profiles were inputted into a fractal analysis program (Rise Co.) by tracing an outline of the picture with a cursor. When the pictures had been inputted, the fractal dimension was calculated.

Statistical analysis Data for the frequency distribution of Ki-67-positive cells and negative cells in 2-D morphometry were analyzed by the Mann-Whitney *U* test. Data for the fractal dimension of each polyp were analyzed by the Kruskal-Wallis rank-sum test. The Bonferroni method was applied to test for the significance of simultaneous multiple comparisons. Statistical significance was defined as $P \leq 0.05$.

RESULTS

3-D reconstruction Fig. 5 illustrates a representative 3-D view of HP. The light microscopic photograph corresponding to this 3-D computer-assisted illustration is shown in Fig. 1. The contour of the apical membrane in HP appears serrate, but the structural complexity is hardly seen in 3-D examination. In addition, Ki-67-positive cells were localized mainly in the bottom of the crypts.

Fig. 6 is a representative computer-assisted 3-D image of TA. The original light microscopic rendition of this 3-D image is shown in Fig. 2. The contour of the apical membrane in TA was smooth, its structure was simple and branching, and glandular budding was not frequently seen. In addition, Ki-67-positive cells were diffusely distributed in the crypts.

Fig. 7 illustrates a representative 3-D view of SA. The original light microscopic appearance is shown in Fig. 3. The contour of the apical membrane in SA appears "serrate," as in HP. Branching and glandular budding are markedly detected in contrast to TA and HP. Ki-67-positive cells were localized mainly at branching points and depressed sites in the serrated epithelium.

2-D morphometry for analyzing the distribution pattern of Ki-67-positive cells In all three SA cases examined, Ki-67-positive cells were more frequently detected on shorter lines drawn between basal and apical membrane compared to Ki-67-negative cells in SA ($P<0.0001$; Fig. 8).

Fractal geometric analysis Linear segments were identified on log-log graphs in the range of 5–50 pixels. The gradients of these segments were considered as the fractal dimensions (Fig. 9). The measured fractal dimension exceeded the topological dimension (one) in all specimens. Results of the fractal dimension in each polyp are summarized in Table I. The fractal dimensions for SA

Fig. 5. An example of a 3-D reconstruction of a hyperplastic polyp, reproduced on a computer display. Glandular lumens (dark brown) shows serrate, but not complicated, branching. Ki-67-positive cells (red) are localized mainly in the bottom of the crypts.

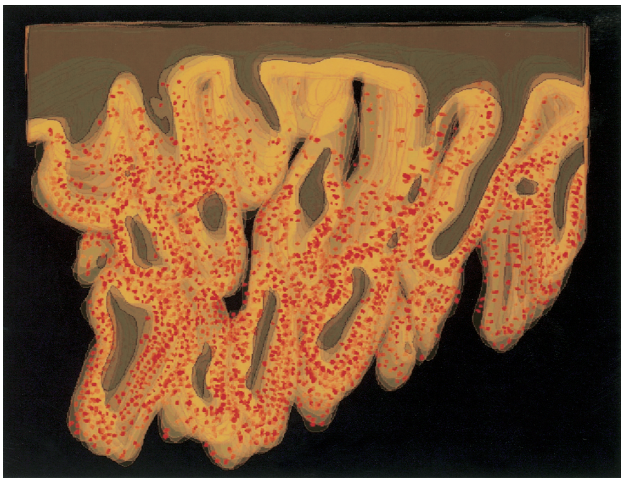

Fig. 6. A representative 3-D reconstruction of a tubular adenoma, reproduced on a computer display. The glandular lumens (dark brown) are oval and smooth. Tubules are closely packed, but not frequently anastomosing adjacent tubules. Ki-67-positive cells (red) are distributed throughout the crypts.

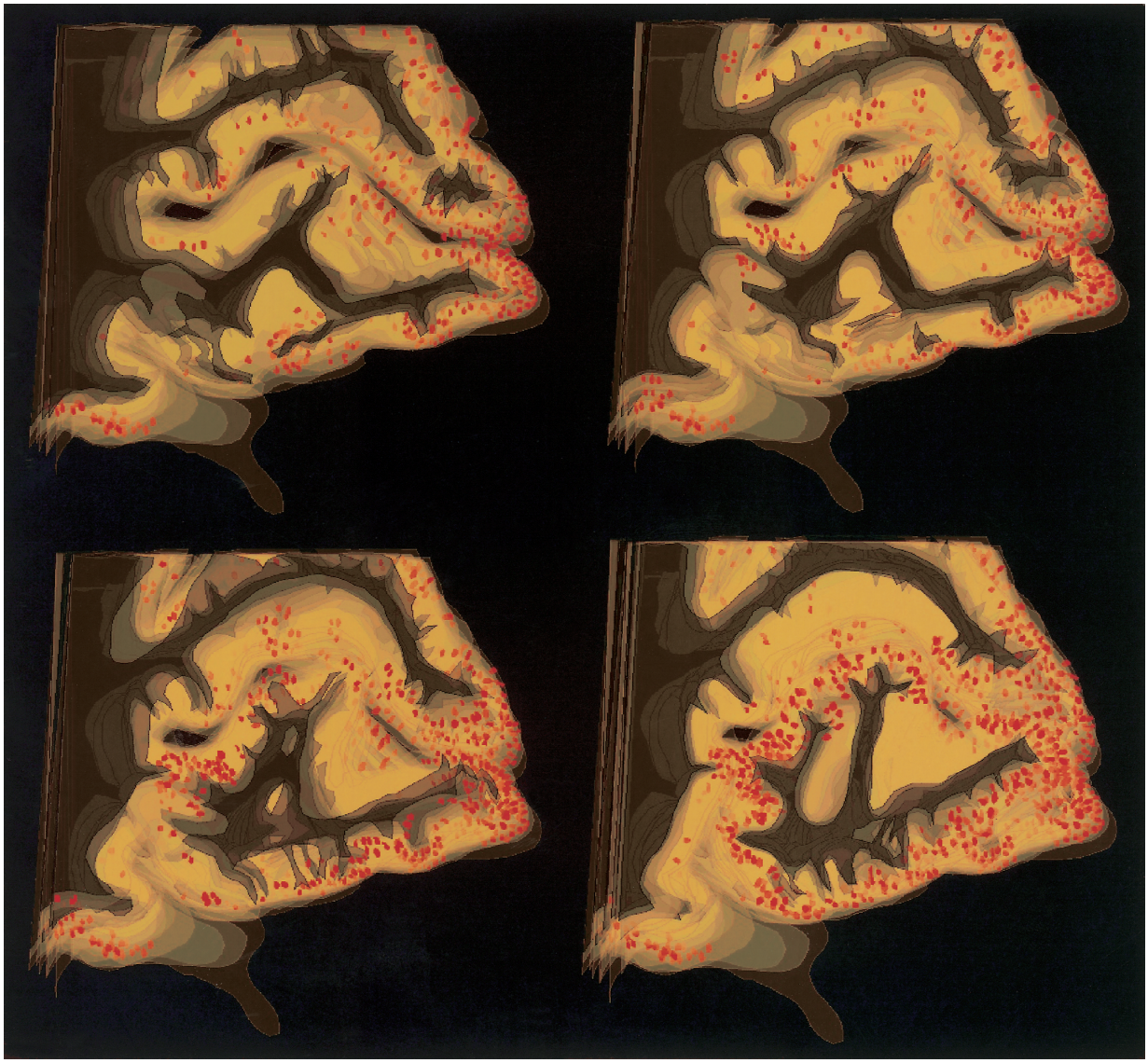

Fig. 7. A representative 3-D reconstruction of a serrated adenoma, reproduced on a computer display. A total of four 3-D pictures are demonstrated by cutting the images into various thicknesses. The glandular lumens (black) demonstrate typical serration, and have multiple connections with adjacent ones, forming a kind of network. Ki-67-positive cells (red) are distributed at branching points and depressed sites of the serrated epithelium.

were significantly higher than that of HP (P=0.0021) or TA (P<0.0001). No significant differences were detected between HP and TA.

DISCUSSION

SA is a relatively newly established morphological entity of colorectal neoplasia.[6] Recently, its clinicopathological[8–10] and immunohistochemical[8, 10, 21] features, as well as genetic findings[22–24] have been reported. However, inconsistent results were obtained among these studies. For instance, the frequencies of p53 nuclear immunoreactivity,[10, 21, 24] or K-ras mutation[22–24] in SA were markedly different among these studies. However, one possible reason for these discrepancies is that histological criteria for SA may be different among laboratories, because the designation SA includes a wide spectrum of colonic lesions, from those similar to hyperplastic polyps to those similar to classical tubular adenoma. In addition, glandular luminal serration is one of the most marked character-

istics of this polyp, but its detailed morphological characteristics are still unclear. Therefore, morphological analysis is required to resolve the difficulties in the assessment of these pathological lesions. We studied 3-D reconstruction models, as well as the distribution patterns for cell-cycle-related nuclear antigen, Ki-67.[25, 26] Quantitative analysis of Ki-67 distribution patterns utilizing 2-D morphometry, and fractal geometric analysis, which has frequently been used in the quantitative analysis of morphometric features, were also performed in assessing the structural characteristics of the pathological lesions investigated in this study.

The 3-D analysis of colorectal polyps in our present study clearly demonstrated distinct structural differences.

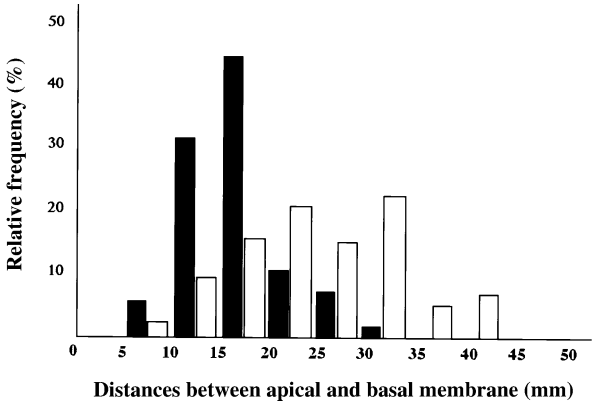

Fig. 8. An example of the frequency distribution of Ki-67-positive and negative cells in a representative case of SA. Ki-67-positive cells (■ black bars) were observed significantly more frequently on shorter lines compared with Ki-67-negative cells (□ white bars).

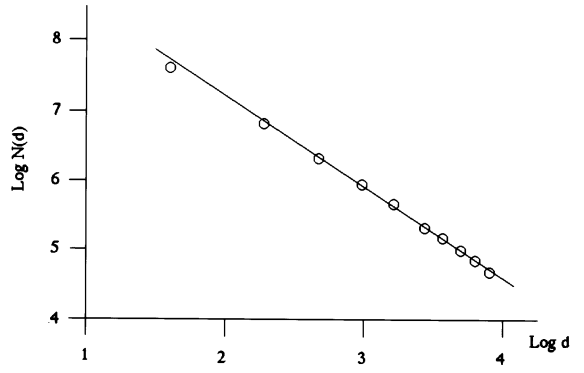

Fig. 9. Log-log graph of box size (pixels) plotted against the number of outline-containing squares showing a single example of a serrated adenoma. The negative slope of the linear part of this plot is taken to be the fractal dimension of this polyp (1.266).

3-D reconstruction of SA revealed frequent branching and glandular budding, which is clearly complicated compared to that of HP and TA. Longacre and Fenoglio-Preiser[6] reported that surface mitotic activity, nuclear pseudostratification, and nuclear cytoplasmic ratios were greater in SA than in HP, but slightly less than in traditional adenoma. These results suggest that cytological or nuclear atypia in SA may place this lesion between HP and TA. However, the degree of structural complexity of SA has not been fully examined in previous studies on SA. The 3-D models in the present study suggest that the structural complexity is more pronounced in SA compared with HP and TA.

In addition, Ki-67 distribution patterns in SA also provided some clues to the complexity and glandular serration of SA. Our previous study demonstrated that the Ki-67-positive rate for SA (30.8%) was intermediate between that of HP (24.2%) and TA (39.5%).[10] Kang and colleagues[21] also reported a similar result. In the present study, the distribution patterns of Ki-67-positive cells seen in 3-D reconstruction models were markedly different among the polyps. Ki-67-positive cells in TA were diffusely distributed in the crypts and those in HP were localized mainly in the bottom of the crypts, while those in SA were localized predominantly in the depressed sites of serrate epithelia. This result has also been confirmed by 2-D

Table I. Fractal Dimensions of SA, TA, and HP

	n	Fractal dimension	
SA	27	1.34±0.08	P=0.0002
TA	19	1.23±0.07	P=0.0369
HP	15	1.28±0.12	

The Bonferroni method was applied to assess the significance of simultaneous multiple comparisons.

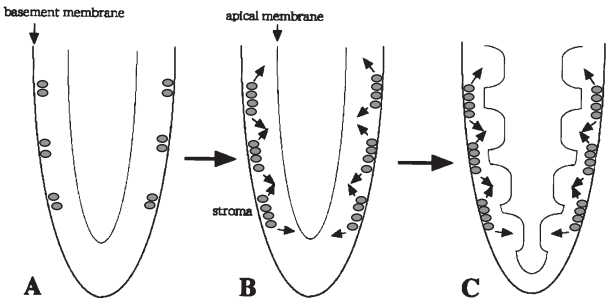

Fig. 10. A model for the formation of characteristic serrated epithelia in SA. A. Proliferative zones are localized at depressed sites of serrated epithelia. B. The epithelia grow not towards along the axis of the crypt, but perpendicularly to the axis. C. This abnormal direction of the epithelial growth may cause the characteristic serration in SA. ● Ki-67 positive cells.

morphometry. From these findings, we propose the following hypothesis on the formation of the serrated epithelia characteristic of SA. Proliferative cells in SA are considered to migrate towards not the surface of the crypt, but instead in abnormal directions. In other words, epithelia in the depressed sites in SA may grow not only along the axis of the crypt, but also perpendicularly to the axis (Fig. 10). Nakamura and colleagues[27] suggested a similar hypothesis. In this case, epithelial growth is considered to be more rapid than adjacent stromal growth in SA. This unequal proliferation rate between the epithelia and adjacent stroma is therefore considered to be involved in the formation of the complicated glandular serration observed in SA. In addition, the unequal rates of proliferation and apoptosis of the epithelia may also contribute to this phenomenon. Further investigations will be needed to clarify these hypotheses.

The structural complexity of SA was also confirmed quantitatively by the fractal dimension. For all diagnostic categories, the measured fractal dimension exceeded the topological dimension, so these polyps fulfill the mathematical definition of fractal structures,[15] which accords with their subjectively self-similar morphology. It is now widely accepted that the fractal dimension is a very useful morphometric discriminant.[28] Fractal geometric analysis has been applied in the analysis of neuronal dendritic arborizations,[29] vascular heterogeneity in the heart,[30] formation of human retinal blood vessels in the kidney,[31] the structure of the bronchial tree,[32, 33] and the distribution and quantification of arterial blood vessels in the kidney.[34, 35] Recently, in the field of pathology, fractal dimensions of the histological structure of colorectal polyps[17] and cell growth patterns in human malignant tumors[36] have been reported. Cross *et al.*[17] have suggested that the fractal dimension is a better way of quantitating polyp shape and is a useful morphometric discriminant among diagnostic categories. Our present study showed that SA also had a fractal structure and the fractal dimension of SA was significantly higher than those of HP and TA. Our findings have demonstrated by quantitative means the structural complexity of SA. Further studies are required to clarify the roles of these complexities in the pathophysiology of these lesions.

ACKNOWLEDGMENTS

The authors appreciate the assistance of the staff at the Cancer Detection Center of Miyagi Cancer Society, Sendai, especially Ms. T. Konno, for providing the paraffin blocks of the polypectomy specimens. This work is, in part, supported by the Grant-in-Aid for Cancer Research 7-1 from the Ministry of Health, habour and Welfare, Japan, a Grant-in-Aid for Scientific Research on Priority Areas (A-11137301) from the Ministry of Education, Culture, Sports, Science and Technology, Japan, a Grant-in-Aid for Scientific Research (B-11470047) from Japan Society for the Promotion of Science, and grants from the Naitou Foundation and Suzukenn Memorial Foundation. The authors appreciate the editorial assistance of Mr. Andrew Darnel, who provided important feedback and critique (Department of Pathology, Tohoku University School of Medicine, Sendai).

(Received September 5, 2001/Revised December 3, 2001/Accepted December 20, 2001)

REFERENCES

1) Arthur, J. F. Structure and significance of metaplastic nodules in the rectal mucosa. *J. Clin. Pathol.*, **21**, 735–743 (1968).
2) Enterline, H. T. Pathology of the gastrointestinal tract: polyps and cancer of the large bowel. *Curr. Top. Pathol.*, **63**, 97–141 (1976).
3) Morson, B. C. Some peculiarities in the histology of intestinal polyps. *Dis. Colon Rectum*, **5**, 337–344 (1962).
4) Fenoglio, C. M., Kaye, G. I., Pascal, R. R. and Lane, H. Definiting the precursor tissue of ordinary large bowel carcinoma : implication for cancer prevention. *Pathol. Annu.*, **12**, 67–116 (1977).
5) Goldman, H., Ming, S. C. and Hickok, D. F. Nature and significance of hyperplastic polyps of the human colon. *Arch. Pathol.*, **89**, 349–354 (1970).
6) Longacre, T. A. and Fenoglio-Preiser C. M. Mixed hyperplastic adenomatous polyps/serrated adenomas. A distinct form of colorectal neoplasia. *Am. J. Surg. Pathol.*, **14**, 524–537 (1990).
7) Watanabe, H., Numazawa, M., Shoji, K., Hiwatashi, N. and Goto, Y. Diagnosis of early cancer of the colon and rectum. *Tohoku J. Exp. Med.*, **129**, 183–195 (1979).
8) Yao, T., Kouzuki, T., Kajiwara, M., Matsui, N., Oya, M. and Tsuneyoshi, M. Serrated adenoma of the colorectum, with reference to its gastric differentiation and its malignant potential. *J. Pathol.*, **187**, 511–517 (1999).
9) Matsumoto, T., Mizuno, M., Shimizu, M., Manabe, T. and Iida, M. Clinicopathological features of serrated adenoma of the colorectum: comparison with traditional adenoma. *J. Clin. Pathol.*, **52**, 513–516 (1999).
10) Iwabuchi, M., Sasano, H., Hiwatashi, N., Masuda, T., Shimosegawa, T., Toyota, T. and Nagura, H. Serrated adenoma : a clinicopathological, DNA ploidy, and immunohistochemical study. *Anticancer Res.*, **20**, 1141–1148 (2000).
11) Yaegashi, H., Takahashi, T. and Kawasaki, M. Microcomputer-aided reconstruction: a system designed for the study of 3-D microstructure in histology and histopathology. *J. Microsc.*, **146**, 55–65 (1987).
12) Nakamura, Y. and Takahashi, T. A computer-aided 3-D

geometry of acute and chronic zonal necrosis: three-D tangent counting applied in an attempt to re-examine the structure of the human liver. *Tohoku J. Exp. Med.*, **184**, 207–227 (1998).
13) Risio, M., Coverlizza, S., Ferrare, A., Candelaresi, G. L. and Rossini, F. P. Immunohistochemical study of epithelial cell proliferation in hyperplastic polyps, adenomas, and adenocarcinomas of the large bowel. *Gastroenterology*, **94**, 899–906 (1988).
14) Johnston, P. G., O'Brien, M. J., Dervan, P. A. and Carney, D. N. Immunohistochemical analysis of cell kinetic parameters in colonic adenocarcinomas, adenomas, and normal mucosa. *Hum. Pathol.*, **20**, 696–700 (1989).
15) Mandelbrot, B. B. "The Fractal Geometry of Nature" (1983). W. H. Freeman, New York.
16) Peitgen, H. O., Jurgens, H. and Saupe, D. "Fractals in the Classroom: Part One-Introduction to Fractals and Chaos" (1992). Springer-Verlag, New York.
17) Cross, S. S., Bury, J. P., Silcocks, P. B., Stephenson, T. J. and Cotton, D. W. K. Fractal geometric analysis of colorectal polyps. *J. Pathol.*, **172**, 317–323 (1994).
18) Peitgen, H. O., Jurgens, H. and Saupe, D. "Chaos and Fractals: New Frontiers of Science," pp. 218–219 (1992). Springer-Verlag, New York.
19) Froyland, J. Fractals. *In* "Introduction to Chaos and Coherence," ed. J. Froyland, pp. 3–8 (1992). Institute of Physics Publishing, Bristol.
20) Gulick, D. Fractals. *In* "Encounters with Chaos," ed. D. Gulick, pp. 188–239 (1992). McGraw-Hill, New York.
21) Kang, M., Mitomi, H., Sada, M., Tokumitsu, Y., Takahashi, Y., Igarashi, M., Katsumata, T. and Okayasu, I. Ki-67, p53, bcl-2 expression of serrated adenomas of the colon. *Am. J. Surg. Pathol.*, **21**, 417–423 (1997).
22) Uchida, H., Ando, H., Maruyama, K., Kobayashi, H., Toda, H., Ogawa, H., Ozawa, T., Matsuda, Y., Sugimura, H., Kannno, T. and Baba, S. Genetic alterations of mixed hyperplastic adenomatous polyps in the colon and rectum. *Jpn. J. Cancer Res.*, **89**, 299–306 (1998).
23) Ajioka, Y., Watanabe, H., Jass, J. R., Yokota, Y., Kobayashi, M. and Nishikura, K. Infrequent K-ras 12 mutation in serrated adenomas of human colorectum. *Gut*, **42**, 680–684 (1998).
24) Hiyama, T., Yokozaki, H., Shimamoto, F., Haruma, K., Yasui, W., Kajiyama, G. and Tahara, E. Frequent p53 gene mutations in serrated adenomas of the colorectum. *J. Pathol.*, **186**, 131–139 (1998).
25) Gerdes, J., Lemke, H., Baisch, H., Wacker, H. H., Schwab, U. and Stein, H. Cell cycle analysis of a cell proliferation-associated human nuclear antigen defined by the monoclonal antibody Ki-67. *J. Immunol.*, **133**, 1710–1715 (1984).
26) Brown, D. C. and Gatter, K. C. Monoclonal antibody Ki-67: its use in histopathology. *Histopathology*, **17**, 489–503 (1990).
27) Nakamura, S., Sato, H. and Sugai, T. Histological analysis of the serrated glands and differential diagnosis of the hyperplastic polyp and serrated adenoma. *Stomach Intestine*, **33**, 843–849 (1998).
28) Cross, S. S. and Cotton, D. W. K. The fractal dimension may be a useful morphometric discriminant in histopathology. *J. Pathol.*, **166**, 409–411 (1992).
29) Caserta, F., Stanley, H. E., Eldred, W. D., Daccord, G., hausman, R. E. and Nittmann, J. Physical mechanisms underlying neurite outgrowth: a quantitative analysis of neuronal shape. *Phys. Rev. Lett.*, **64**, 95–98 (1990).
30) van Beek, J. H. G. M., Bassingthwaighte, J. B. and King, R. B. A fractal vascular network explains regional flow heterogeneity. *Biophys. J.*, **49** (Suppl.), 401 (1988).
31) Family, F., Masters, R. B. and Plat, D. E. Fractal pattern formation in human retinal vessels. *Physica. D.*, **38**, 98–103 (1989).
32) West, B. J., Bhargava, V. and Goldberg, A. L. Beyond the principle of similitude: renormalization in the bronchial tree. *J. Appl. Physiol.*, **60**, 189–197 (1986).
33) West, B. J. and Goldberg, A. L. Physiology in fractal dimensions. *Am. Sci.*, **75**, 354–365 (1987).
34) Sernets, M., Wubbeke, J. and Wlczek, P. Three-dimensional image analysis and fractal characterization of kidney arterial vessels. *Physica. A.*, **191**, 13–16 (1989).
35) Cross, S. S., Start, R. D., Silcocks, P. B., Bull, A. D., Cotton, D. W. and Underwood, J. C. Quantitation of the renal arterial tree by fractal analysis. *J. Pathol.*, **170**, 479–484 (1993).
36) Vilela, M. J., Martins, M. L. and Boschetti, S. R. Fractal patterns for cells in culture. *J. Pathol.*, **177**, 103–107 (1995).